Brushless Doubly-Fed Induction Machines: Magnetic Field Modelling

T. D. Strous, N.H. van der Blij, H. Polinder, J. A. Ferreira

***Abstract* – The brushless DFIM is a complex machine type. Though never commercially exploited, it has a great potential as generator system in large-scale wind turbines. This paper develops an analytical magnetic field model for the brushless DFIM. Since the brushless DFIM rotor construction has a rich space harmonic spectrum, attention is paid to the effects of winding space-harmonics. The developed model is validated by FE calculations. With use of the developed model, the brushless DFIM operating principles are considered from the point of view of the magnetic field.**

***Index Terms*—Brushless Doubly-Fed Machine (BDFM), DFIG, Cross coupling, Magnetic field Model, Space Harmonics, Nested-loop Rotor, Torque Ripple.**

I. Introduction

PRIOR to the development of semi-conductor power-electronics, it was difficult efficiently controlling the speed of AC machines over a large operating area. Already in 1897 Steinmetz in the U.S. and Görges in Germany independently devised the cascade system of control, in an attempt to provide more control flexibility for induction machines [1]. Their principle of connecting two wound-rotor induction machines in cascade would eventually evolve in what is now called the brushless Doubly-Fed Induction Machine (DFIM). This complex machine type, though never commercially exploited, has gained increased research interest in recent years. This is because of its potential as generator system in large scale wind-turbines [2]. The advantages of employing a Brushless DFIM include:

- The use of a partially rated Power Electronic (PE) converter; reducing time harmonic distortion, PE losses and PE cost, while enabling power factor control.
- No brush gear and slip rings; increasing robustness and reliability while decreasing the need for maintenance.
- A low speed machine type; enables the reduction of the number of gear stages, which increases reliability.
- Improved capabilities to comply with current grid-code requirements.

The motion of the magnetic field in a brushless DFIM is not a simple rotation as in other types of AC machines. Therefore more complex analysis is required. This paper focusses on developing a detailed analytical analysis for brushless DFIM's. By considering the brushless DFIM rotor as a balanced poly-phase system, methods well known in rotating-field theory [3] can be applied. This results in a simplified magnetic field model, that provides insight in the machines basic operating principles.

The research leading to these results has received funding from the European Union's Seventh Framework Programme managed by REA – Research Executive Agency (FP7/2007_2013) under Grant Agreement N.315485.

T. D. Strous, N.H. van der Blij, H. Polinder and J. A. Ferreira are with the Department of Electrical Sustainable Energy, Delft University of Technology, The Netherlands (e-mail: t.d.strous@tudelft.nl)

Some other references can be found on magnetic field modelling in brushless DFIM's. One of the most rigorous analytical magnetic field models can be found in [4]. Although only the main harmonic magnetic field components are evaluated, the paper provides good insight in the operating mechanisms of the brushless DFIM. In [5] an alternative magnetic field model is derived. Here attention is paid to the evaluation of rotor winding space-harmonics in the brushless DFIM magnetic field.

Winding space-harmonics are more dominant in the Brushless DFIM than in the more traditional machine-types. Therefore, this paper includes harmonic analysis in its analytical magnetic field model derivation. By employing a common fundamental pole-pitch for all windings, as is done in [6] for cage induction machines, a simplified analysis of the space-harmonic coupling between stator and rotor magnetic field is presented.

Finally the derived model is validated by Finite Element (FE) calculations and the brushless DFIM magnetic field is evaluated, providing more insight in its operating principles.

II. Theoretical Development

A. Brushless DFIM Operating Principles

The brushless DFIM operating principles are based on the superposition of two stator rotating magnetic fields. Those stator rotating magnetic fields are produced by two sets of poly-phase windings, with no direct magnetic coupling between them [7]. A special nested-loop rotor structure ensures coupling with both magnetic field components, hence the stator windings are magnetically cross-coupled [8]. One stator-winding, the power-winding, has p_p pole-pairs and is connected directly to the grid. The other stator-winding, the control-winding, has p_c pole-pairs. The control-winding is connected to a (partially rated) PE-converter. Both stator-winding main space-harmonic magnetic field components, induce time-harmonic voltages in the rotor, with respective frequencies $\omega_{re(pp)}$ and $\omega_{re(pc)}$:

$$\omega_{re(p_p)} = \omega_{pe} - p_p\,\omega_m \quad (1)$$

$$\omega_{re(p_c)} = \omega_{ce} + p_c\,\omega_m \quad (2)$$

For brushless DFIM synchronous operation the voltage induced in the rotor nested-loops, by the power-winding magnetic field, must match the voltage induced by the control-winding magnetic field. Therefore the induced voltages must have the same frequency ($\omega_{re(pp)} = \omega_{re(pc)}$) and phase-delay between consequent rotor nests [4]. For the frequency to be equal (3) must hold, which is derived from (1) and (2):

$$\omega_m = \frac{\omega_{pe} - \omega_{ce}}{p_p + p_c} \quad (3)$$

978-1-4799-4389-0/14/$31.00 ©2014 IEEE

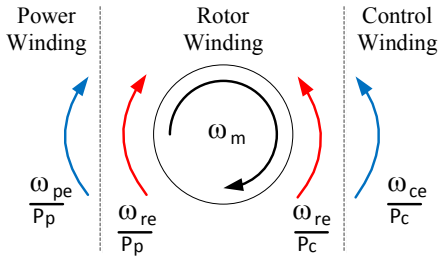

Fig. 1. Brushless DFIM synchronous operation: rotational directions of main harmonic magnetic field components.

For the phase-delay between consequent rotor nests to be equal, the number of rotor nests N_{nest} must be equal to the number of power- and control-winding pole-pairs added. The rotor will then produce two main harmonic rotating-field components, that couple to both the power- and control-winding fields, as is schematically represented in figure 1.

B. Brushless DFIM Modelling

This work considers brushless DFIM's with two balanced poly-phase stator-windings that do not magnetically couple [7]. Further, nested-loop rotor structures are considered. For the brushless DFIM the nested-loop rotor construction is considered favourable over other rotor constructions [9]. In order to reduce the complexity of this analytical model, the following simplifying assumptions are used, which are common to analytical machine design:

- Slotting is neglected, assuming an effective air-gap length and infinitely small conductors in the air-gap.
- The magnetic field crosses the air-gap in radial direction.
- Permeability μ_{Fe} of the iron parts is considered infinite.
- Machine end effects are neglected.

For further modelling, harmonic analysis is used to determine the interaction of winding space-harmonic field components. The windings in the machine can therefore be considered as infinite summations of sinusoidal space-harmonic sheet conductor distributions in the air-gap. A common 'fundamental' harmonic component is chosen, corresponding to a 2-pole wave. Therefore, a space-harmonic field component k can be considered as a k pole-pair field. This simplifies identification of the space-harmonic components from different windings that interact with each other, considering that only space-harmonic components with the same pole-pitch interact [6].

C. The Stator Magnetic Field

Under the given set of assumptions, a stator phase-winding conductor distribution $C_{s,m}$ in (conductors/m), corresponding to one stator phase-winding m, as function of stator position angle θ^s, can mathematically be represented by an infinite summation of sinusoidal space-harmonic sheet conductor distributions, using a Fourier-series representation:

$$C_{s,m}(\theta^s) = \frac{1}{2}\sum_{k=-\infty}^{\infty}\hat{C}_{s(k)}\cos\left(k\theta^s - \frac{k}{p}\beta_m\right) \tag{4}$$

$$\Rightarrow \quad \beta_m = (m-1)\frac{2\pi}{N_{ph}} \qquad \forall\ m \in \mathbb{N}\cap\{1:N_{ph}\}$$

$$\Rightarrow \quad \hat{C}_{s(k)} = \frac{1}{r_{si}}\frac{2}{\pi}n_c\,k_{w(|k|)}\,p\,q$$

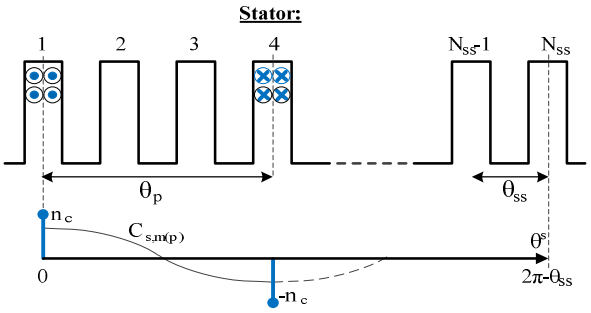

Fig. 2. Brushless DFIM stator phase-winding, and its winding distribution.

Here N_{ph} is the number of phase windings, r_{si} is the stator inner radius, n_c is the number of phase-winding conductors per slot and k_w is the winding factor [10]. Figure 2 provides a visual representation of a stator phase-winding conductor distribution according to (4), with an arbitrary number of pole-pairs p and one slot per pole per phase q.

Now consider a set of perfectly balanced sinusoidal stator currents $i_{s,m}$(A), flowing through the stator phase-windings as defined by (4):

$$i_{s,m}(t) = \hat{i}_s\cos(\omega_{se}t - \phi_m - \varphi_s) \tag{5}$$

$$\Rightarrow \quad \phi_m = (m-1)\frac{2\pi}{N_{ph}} \qquad \forall\ m \in \mathbb{N}\cap\{1:N_{ph}\}$$

Here ω_{se} is the radial frequency of the currents in the corresponding stator-winding, while φ_s represent a phase-shift for the stator-winding phase-currents.

An axially directed linear surface current density distribution, corresponding to one phase-winding is found by the product of the phase-winding conductor distribution of (4) and the current of (5) flowing through. Principles well known to rotating-field theory [3] are then used to determine the total stator-winding linear surface current density distribution J_s^s in (A/m). Consisting of a summation of harmonic rotating wave components:

$$J_s^s(\theta^s,t) = \sum_{k=-\infty}^{\infty}\hat{J}_{s(k)}\cos(\omega_{se}t - k\theta^s - \varphi_s) \tag{6}$$

$$\Rightarrow \quad \hat{J}_{s(k)} = \frac{N_{ph}}{2}\hat{C}_{s(k)}\,\hat{i}_s$$

Using (6) to model both the Brushless DFIM power- and control-winding linear surface current density, k should be an element of (7) when considering the power-winding and an element of (8) when considering the control-winding:

$$PW \Rightarrow k = k_p \in p_p(1-2nN_{ph}) \qquad \forall\ n \in \mathbb{Z} \tag{7}$$

$$CW \Rightarrow k = k_c \in p_c(2nN_{ph}-1) \qquad \forall\ n \in \mathbb{Z} \tag{8}$$

The magnetic field B_s^s in the air-gap, produced by a stator-winding surface current density, is obtained by the application of Ampère's law around the contour shown in figure 3.

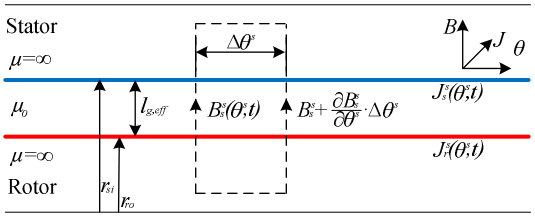

Fig. 3. Linearized view of brushless DFIM model: Application of Ampère's law.

This results into (9):

$$\frac{\partial B_s^s}{\partial \theta^s}(\theta^s,t) = \frac{\mu_0}{l_{g,eff}} r_{si} J_s^s \quad (9)$$

Here $l_{g,eff}$ is the effective air-gap length, after compensation for the neglect of slotting [10]. Combining (6)-(9) results into an infinite series of stator-winding space-harmonic rotating flux-density waves:

$$B_s^s(\theta^s,t) = \sum_{k=-\infty}^{\infty} \hat{B}_{s(k)} \sin\left(\omega_{se} t - k\theta^s - \varphi_s\right) \quad (10)$$

$$\Rightarrow \quad \hat{B}_{s(k)} = -\frac{N_{ph}}{2}\frac{\mu_0}{k\, l_{g,eff}} r_{si}\, \hat{C}_{s(k)}\, \hat{i}_s$$

Rotating wave components traveling in positive/negative direction are also represented by positive/negative space-harmonic numbers k.

Figure 4 shows the total stator magnetic field distribution $B^s_{s,tot}$, including the main space-harmonic field components of the power- and control-winding, for an arbitrary machine with p_p=2 and p_c=3.

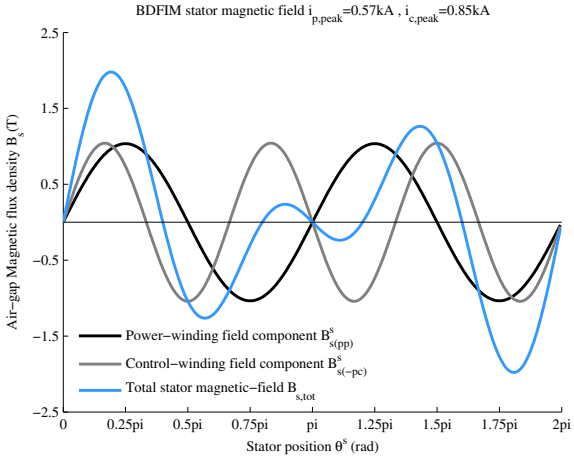

Fig. 4. Brushless DFIM stator magnetic field distribution, including the main harmonic field components of the power- and control-winding.

D. The Rotor Magnetic field

The rotor nested-loop construction can be considered as a balanced poly-phase system, where the number of phases is equal to the number of rotor nests N_{nest}. This is possible since the currents induced in the nest-loops, by the stator magnetic field, have the same amplitude and phase delay between consequent rotor nests, during stable operation. However, the currents between loops in the same nests do not have the same amplitude. Therefore they could be considered as belonging to another poly-phase winding. Hence, the rotor nested-loop construction consists of q_r poly-phase windings, with each N_{nest} phases, where q_r is the number of loops per nest.

Consider the conductor distribution $C_{r,nl}$ in (conductors/m) of a single phase of one rotor poly-phase winding, as function of rotor position angle θ^r. This corresponds to the conductor distribution of a single loop l in a nest n. The conductor distribution can mathematically be represented by an infinite summation of sinusoidal rotor space-harmonic k_r sheet conductor distributions in the air-gap, using a Fourier-series representation:

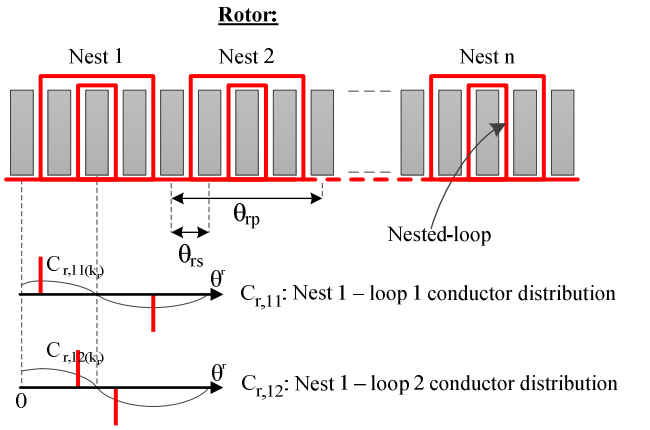

Fig. 5. Brushless DFIM rotor nested-loop construction and the winding distribution of a single rotor phase.

$$C_{r,nl}(\theta^r) = \frac{1}{2}\sum_{k_r=-\infty}^{\infty} \hat{C}_{r,l(k_r)} \sin\left(k_r\left(\theta^r - \beta_{r,n}\right)\right) \quad (11)$$

$$\Rightarrow \quad \beta_{r,n} = (2n-1)\frac{\pi}{N_{nest}} \qquad \forall\ n \in \mathbb{N} \cap \{1 : N_{nest}\}$$

$$\Rightarrow \quad \hat{C}_{r,l(k_r)} = \frac{1}{r_{ro}}\frac{1}{\pi} 2\sin\left(|k_r|\gamma_{r,l}\,\theta_{rp}\right)$$

Here r_{ro} is the rotor outer radius, $\gamma_{r,l}$ is the rotor loop span as factor of the full rotor nest pitch θ_{rp}. Figure 5 provides a visual representation of the rotor nested-loop construction and the conductor distribution as described in (11)

The phase current $i_{r,nl}$ through a rotor nest loop can be described as a summation of time-harmonic rotor currents, induced by the space-harmonic components k of the stator magnetic fields (power- and control-winding fields):

$$i_{r,nl}(t) = \sum_{k=-\infty}^{\infty} \hat{i}_{r,l(k)} \cdot \cos\left(\omega_{re(k)} t - \phi_{r,n} - \varphi_{r,l(k)}\right) \quad (12)$$

$$\Rightarrow \quad \phi_{r,n} = k\beta_{r,n}$$

The derivation of the current peak value $\hat{\imath}_{r,l(k)}$ and the phase-delay $\varphi_{r,l(k)}$ will follow in section II F. The time-harmonic frequencies $\omega_{re(k)}$ are given by (13):

$$\omega_{re(k)} = \begin{cases} \omega_{pe} - k\omega_m & \forall\ k \in k_p = p_p\left(1 - 2nN_{ph}\right) \\ \omega_{ce} - k\omega_m & \forall\ k \in k_c = p_c\left(2nN_{ph} - 1\right) \\ & \forall\ n \in \mathbb{Z} \end{cases} \quad (13)$$

Considering the brushless DFIM rotor as a set of multiple poly-phase windings, enables the use of rotating-field theory principles for determining the rotor linear surface current density distribution J_r^r in (A/m). This results in an infinite series of rotating linear surface current density waves:

$$J_r^r(\theta^r,t) = \sum_{l=1}^{q_r} J_{r,l}^r \quad (14)$$

$$J_{r,l}^r(\theta^r,t) = \sum_{k=-\infty}^{\infty}\sum_{k_r=-\infty}^{\infty} \hat{J}_{r,l(k,k_r)} \sin\left(\omega_{re(k)} t - k_r\theta^r - \varphi_{r,l(k)}\right) \quad (15)$$

$$\Rightarrow \hat{J}_{r,l(k,k_r)} = \mp\frac{N_{nest}}{2}\hat{C}_{r,l(k_r)}\,\hat{i}_{r,l(k)} \qquad \forall\ k_r \in k + nN_{nest}$$

$$\forall\ k \in \{k_p \cup k_c\}\ \forall\ n \in \mathbb{Z}$$

In (15) $\hat{J}_{r,l(k,k_r)}$ is positive if $k_r \in \left(k \pm (2n+1)N_{nest}\right)\ \forall\ n \in \mathbb{N}$.

By applying Ampère's law, the rotor flux-density distribution $B_r{}^r$ is found and presented as an infinite series of rotating field waves:

$$B_r^r(\theta^r,t) = \sum_{l=1}^{q_r} B_{r,l}^r(\theta^r,t) \quad (16)$$

$$B_{r,l}^r(\theta^r,t) = \sum_{k=-\infty}^{\infty}\sum_{k_r=-\infty}^{\infty} \hat{B}_{r,l(k_r,k)} \cos\left(\omega_{re(k)}t - k_r\theta^r - \varphi_{r,l(k)}\right) \quad (17)$$

$$\Rightarrow \hat{B}_{r,l(k,k_r)} = \frac{N_{nest}}{2}\frac{\mu_0}{k_r \cdot l_{g,eff}} r_{ro}\, \hat{J}_{r,l(k_r,k)} \qquad \forall\ k_r \in k + nN_{nest}$$

Again, positive/negative space-harmonic numbers k_r also represent rotating wave components traveling in positive/negative direction. The rotor magnetic field distribution has two main harmonic field components, $k_r=p_p$ and $k_r=-p_c$, which have the same frequency ω_{re}. They couple to the main harmonic field components of the stator's power- and control-winding.

E. Magnetic Field Coupling: Flux Linkage

The amount of flux passing through a winding is called the flux-linkage. The flux can be either induced by the winding itself or by another winding. The former two sub-sections considered the stator and rotor magnetic field distributions. This section focusses on the flux-linkage of those two magnetic field components with themselves and with each other.

The brushless DFIM total magnetic field in the air-gap can be considered as the superposition of power-winding, control-winding and rotor magnetic field components, as described by (10) and (16). According Faraday's induction law, a time-varying flux-linkage λ will induce a voltage. The induced voltages $u_{ss,m}$, by the total stator magnetic-field, in the stator-phase windings, is therefore given by:

$$u_{ss,m}(t) = \frac{d\lambda_{ss,m}^s}{dt} \quad (18)$$

$$\Rightarrow \lambda_{ss,m}^s(t) = l_{stk}\int_{\theta^s=0}^{2\pi}\int B_s^s\, r_{si} d\theta^s\ C_{s,m}\, r_{si} d\theta^s$$

Here l_{stk} is the machine stack length in axial direction. Now considering there is no flux-linkage between power-winding and control-winding, (4) and (10) can be substituted into (18), resulting after rewriting into:

$$u_{ss,m}(t) = \sum_{k=-\infty}^{\infty} \hat{u}_{ss(k)} \sin\left(\omega_{se}t - \frac{k}{p}\beta_m - \varphi_s\right) \quad (19)$$

$$\Rightarrow \hat{u}_{ss(k)} = \omega_{se}\, M_{s(k)}\, \hat{i}_s$$

$$\Rightarrow L_{s(k)} = \frac{N_{ph}}{2}\hat{C}_{s(k)}{}^2\, \pi\, l_{stk}\, r_{si}^3 \frac{\mu_0}{l_{g,eff}}\frac{1}{k^2}$$

$L_{s(k)}$ is the stator-winding (1-phase equivalent) inductivity, due to the k^{th} stator winding space-harmonic component.

The total stator magnetic field also induces a voltage in the loops of the rotor nests. By applying Faraday's induction law, the induced voltage $u_{rs,nl}$ in the loop of a rotor nest can be found:

$$u_{rs,nl}(t) = \frac{d\lambda_{rs,nl}^r}{dt} \quad (20)$$

$$\Rightarrow \lambda_{rs,nl}^r(t) = l_{stk}\int_{\theta^r=0}^{2\pi}\int B_s^r\, r_{ro} d\theta^r\, C_{r,nl}\, r_{ro} d\theta^r$$

The stator magnetic field in (20) is considered from the rotor reference frame:

$$\theta^s = \theta^r + \omega_m t + \gamma_{shift} \quad (21)$$

γ_{shift} is the position shift of the rotor with respect to the stator at time $t = 0$. Substitution of (13) and (21) into (10) provides the stator magnetic field distribution $B_s{}^r$ in the rotor reference frame:

$$B_{s(k)}^r(\theta^r,t) = \sum_{k=-\infty}^{\infty} \hat{B}_{s(k)} \sin\left(\omega_{re(k)}t - k\theta^r - k\gamma_{shift} - \varphi_s\right) \quad (22)$$

Both space-harmonic components corresponding to the power- and the control-winding are included in (22). Substitution of (11) and (22) into (20) gives the voltage $u_{rs,nl}$ induced by the total stator magnetic field, in loop l of rotor nest n:

$$u_{rs,nl}(t) = \sum_{k=-\infty}^{\infty} \hat{u}_{rs,l(k)} \cos\left(\omega_{re(k)}t - k\beta_{r,n} - k\gamma_{shift} - \varphi_s\right) \quad (23)$$

$$\Rightarrow \hat{u}_{rs,l(k)} = \omega_{re(k)}\, M_{rs,l(k)}\, \hat{i}_s$$

$$\Rightarrow L_{rs,l(k)} = \frac{N_{ph}}{2}\hat{C}_{s(k)}\,\hat{C}_{r,l(k)}\,\pi\, l_{stk}\, r_{si}\, r_{ro}^2 \frac{\mu_0}{l_{g,eff}}\frac{1}{k^2}$$

Last there is the flux-linkage of the rotor magnetic-field with the rotor-windings. The induced voltage $u_{rr,nl}$ in the phases of the rotor field-windings (in a loop of a rotor nest) is derived according:

$$u_{rr,nl}(t) = \frac{d\lambda_{rr,nl}^r}{dt} \quad (24)$$

$$\Rightarrow \lambda_{rr,nl}^r(t) = l_{stk}\int_{\theta^r=0}^{2\pi}\int B_r^r\, r_{ro} d\theta^r\ C_{r,nl}\, r_{ro} d\theta^r$$

Substitution of (11) and (16) into (24) gives the voltage $u_{rr,nl}$ induced by the total rotor magnetic-field, in loop l of rotor nest n:

$$u_{rr,nl}(t) = -\sum_{k=-\infty}^{\infty}\sum_{k_r=-\infty}^{\infty} \hat{u}_{rrl(k,k_r)} \sin\left(\omega_{re(k)}t - k_r\beta_{r,n} - \varphi_{r,l(k)}\right)$$

$$\Rightarrow \hat{u}_{rrl(k,k_r)} = \omega_{re(k)}\sum_{l_2=1}^{q_r}\left(M_{rl,l_2(k_r)}\,\hat{i}_{r,l_2(k)}\right) \quad (25)$$

$$\Rightarrow L_{rl,l_2(k_r)} = \frac{N_{nest}}{2}\hat{C}_{r,l(k_r)}\,\hat{C}_{r,l_2(k_r)}\,\pi\, l_{stk}\, r_{ro}^3 \frac{\mu_0}{l_{g,eff}}\frac{1}{k_r^2}$$

Using the inductivities derived in (19),(23) and (25) it is possible to schematically represent the brushless DFIM by a simplified single phase equivalent circuit. This is done by making use of the phase symmetry present in both the stator windings as well as in the rotor structure. Figure 6 shows such a circuit. Here only the coupling between main harmonic field components is taken into account. The field components other than the main harmonic components add up to the leakage inductivities.

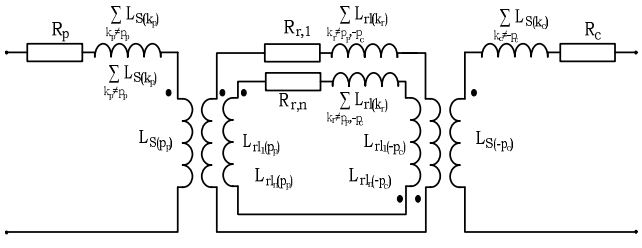

Fig. 6. Brushless DFIM simplified single-phase equivalent circuit representation, including the main space-harmonic field components.

F. The Rotor Currents

The currents in the rotor nested loops $i_{r,nl}$ are powered by the voltage induced by the total magnetic field in the air-gap. Applying Kirchhoff's voltage law, the voltage sum in a loop of a rotor nest must be zero:

$$0 = \sum_{k=-\infty}^{\infty}\left(u_{rs,nl(k)} + \sum_{k_r=-\infty}^{\infty}\left(u_{rr,nl(k,k_r)} - i_{r,nl(k)}R_{r,l}\right)\right) \quad (26)$$

Rewriting equation (26), and substituting (23) and (25), results into:

$$u_{rs,nl(k)}(t) = i_{r,nl(k)}\,R_{r,l} + \sum_{k_r=-\infty}^{\infty}\sum_{l_2=1}^{q_r}\left(L_{rl,l_2(k_r)}\frac{di_{r,nl_2(k)}}{dt}\right) \quad (27)$$

It is clear that the current in one nest-loop also depends on the currents in the other loops. For a rotor with q_r loops per nest this yields q_r equations with q_r unknowns. To determine the rotor currents, (27) is rewritten in exponential form, using complex phasors:

$$\Re\left[\underline{u}_{rs,nl(k)}\,e^{j\omega_{re(k)}}\right] = \quad (28)$$

$$\Re\left[\left(\underline{i}_{r,nl(k)}\,R_{r,l} + j\omega_{re(k)}\sum_{k_r=-\infty}^{\infty}\sum_{l_2=1}^{q_r}\left(L_{rl,l_2(k_r)}\,\underline{i}_{r,nl_2(k)}\right)\right)e^{j\omega_{re(k)}}\right]$$

$$\Rightarrow \quad \underline{i}_{r,nl(k)} = \hat{i}_{r,nl(k)}\,e^{-j\left(k\beta_{r,n}+\varphi_{r,l(k)}\right)}$$

$$\Rightarrow \quad \underline{u}_{rs,nl(k)} = \hat{u}_{rs,nl(k)}\,e^{-j\left(k\beta_{r,n}+k\gamma_{shift}+\varphi_s\right)}$$

Then a matrix equation is set-up to solve at once, for all the rotor loop currents of induced time-harmonic order k:

$$\begin{bmatrix}\underline{i}_{r,n1(k)}\\ \underline{i}_{r,n2(k)}\\ \vdots\\ \underline{i}_{r,nq_r(k)}\end{bmatrix} = \left[\mathbf{R_r} + j\omega_{re(k)}\sum_{k_r=-\infty}^{\infty}\mathbf{L_{r(k_r)}}\right]^{-1}\cdot\begin{bmatrix}\underline{u}_{rs,n1(k)}\\ \underline{u}_{r,n2(k)}\\ \vdots\\ \underline{u}_{r,nq_r(k)}\end{bmatrix} \quad (29)$$

$$\Rightarrow \quad \mathbf{R_r} = \begin{bmatrix}R_{r,1} & 0 & \cdots & 0\\ 0 & R_{r,2} & \cdots & 0\\ \vdots & \vdots & \ddots & \vdots\\ 0 & 0 & \cdots & R_{r,q_r}\end{bmatrix}$$

$$\Rightarrow \quad \mathbf{L_{r(k_r)}} = \begin{bmatrix}L_{rl_1(k_r)} & L_{rl_1,l_2(k_r)} & \cdots & L_{rl_1,l_{q_r}(k_r)}\\ L_{rl_1,l_2(k_r)} & L_{rl_2(k_r)} & \cdots & L_{rl_2,l_{q_r}(k_r)}\\ \vdots & \vdots & \ddots & \vdots\\ L_{rl_1,l_{q_r}(k_r)} & L_{rl_2,l_{q_r}(k_r)} & \cdots & L_{rl_{q_r}(k_r)}\end{bmatrix}$$

G. Torque Generation

Application of the Lorentz-force equation [10], provides the electro mechanic torque T_e exerted on the rotor surface:

$$T_e(t) = r_{ro}\iint\left(J_r^r\left(B_s^r + B_r^r\right)\right)dS_{rotor} \quad (30)$$

Equation (30) contains the brushless DFIM main torque components, as well as the torque ripple due to winding space-harmonics and rotor time-harmonics. When neglecting the effect of time-harmonic rotor currents, other than the main harmonic rotor current components, (30) can be rewritten after substitution of (14) and (22). This results into:

$$T_e(t) = l_{stk}\,r_{ro}^{\,2}\sum_{k=-\infty}^{\infty}\sum_{k_r=-\infty}^{\infty}\int_{\theta^r=0}^{2\pi}\left(J^r_{r(k=p_p,k_r)} + J^r_{r(k=-p_c,k_r)}\right)B^r_{s(k)}\,d\theta^r \quad (31)$$

$$\Rightarrow \quad T_{e(k_r)} = \pm\pi\,l_{stk}\,r_{ro}^{\,2}\,\hat{B}_{s(k_r)}\sum_{l=1}^{q_r}\left(\hat{J}_{r,l(k=p_p,k_r)} + \hat{J}_{r,l(k=-p_c,k_r)}\right)\cdot$$

$$\cos\left(\left(\omega_{re(p_p)} \mp \omega_{re(k_r)}\right) + k_r\gamma_{shift} - \varphi_{r,nl(k_r)}\right)$$

$$\forall\ k_r \in \left|p_p + nN_{nest}\right| \cap \left|p_p\left(1-2nN_{ph}\right) \cup p_c\left(2nN_{ph}-1\right)\right|$$

In (31), $T_{e(kr)}$ is negative if $k_r \in \left(p_p + nN_{nest}\right) \cap \left(-p_p\left(1-2nN_{ph}\right) \cup p_c\left(1-2nN_{ph}\right)\right)\ \forall\, n \in \{\mathbb{Z} : n \neq 0\}$

From (31) it is clear that aside from the main Torque, also additional torque ripple components are produced due to the winding space-harmonics. These ripple torque components have rotational frequencies of $\omega_{re(pp)} - \omega_{re(kr)}$.

III. Model Validation

The developed analytical brushless DFIM magnetic field model is applied to the brushless DFIM design presented in Table I. The calculation results are then validated using a FE model of the brushless DFIM, developed in Comsol. A comparison is made between the analytically calculated and the FE calculated magnetic field distribution in the air-gap in radial direction. Further, the resulting mean torque T_{mean} is compared.

TABLE I:
Brushless DFIM Design

Construction Parameters			
Number of phases	N_{ph}	3	
Number of pole-pairs	p_p , p_c	4 , 6	
Number of stator slots	N_{ss}	72	
Number of rotor nests	N_{nest}	10	
Number of loops per nest	q_r	4	
Geometric Parameters			
Axial stack length	l_{stk}	1.596	m
Air-gap length	l_g	1.5	mm
Stator outer radius	r_{so}	0.83	m
Stator inner radius	r_{si}	0.67	m
Rotor inner radius	r_{ri}	0.58	m
Evaluated operating point			
Rotational speed	ω_m	37.7	rad/s
Maximum slot current density	$J_{p,slot}$, $J_{c,slot}$	1 , 1	A/mm^2
Initial position shift	γ_{shift}	$(90/N_{nest})$	°
Evaluation time period	T_{eval}	$(2\pi/\omega_{re})$	s
Mean Torque over one time period T_{eval}			
Analytical calculation	$T_{e,mean}$	38.6	kNm
FEM calculation	$T_{e,mean}$	37.2	kNm

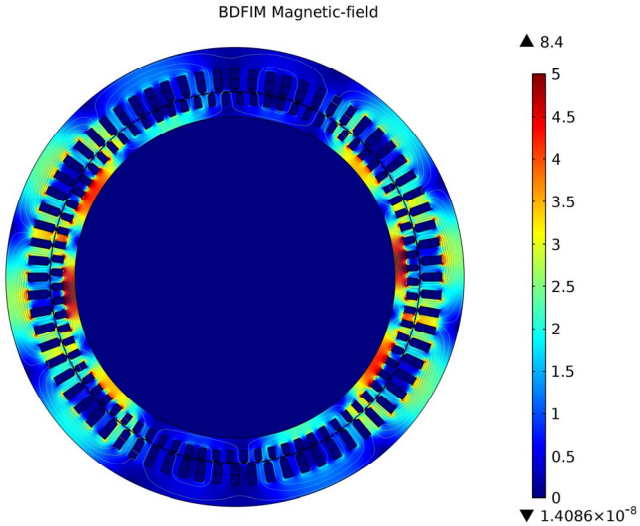

Fig. 7. Brushless DFIM 2D flux density distribution.

Figure 7 presents the brushless DFIM FE model, with the resulting 2D flux density distribution in the machine. Figure 8 presents the resulting air-gap magnetic field distributions of both the analytical and the FE calculation. Both models use perfect sinusoidal currents as input for the power- and control-winding. Further, infinite steel permeability μ_{Fe} is assumed in both models. The FE calculation does include the effect of time-harmonic rotor-currents, induced by the magnetic field. These have been neglected in the analytical results. Further differences between the analytical and FE calculation can be contributed to the negligence of slotting-effects in the analytical model.

The model validation shows that the analytical derived brushless DFIM magnetic field model is able to determine the air-gap magnetic field distribution with reasonable accuracy. Derived from the magnetic field distribution is the mean torque, which is predicted with good accuracy.

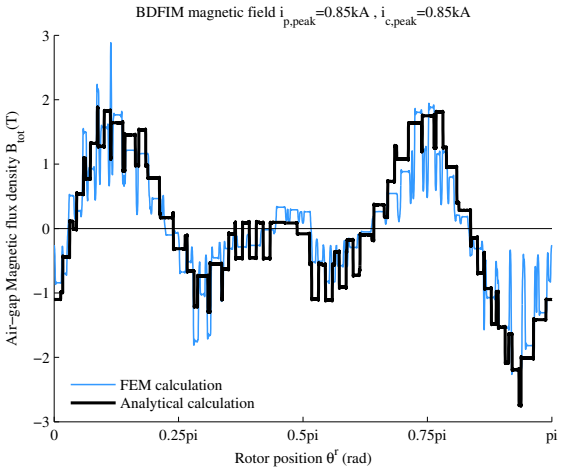

Fig. 8. Brushless DFIM magnetic field distribution in the air-gap in radial direction at an arbitrary moment.

IV. Discussion

A. Brushless DFIM Operating Principles

The derived magnetic-field model provides additional insight in the brushless DFIM operating principles. Figure 9 presents the main harmonic stator and rotor magnetic field components, from a rotor reference frame, for an arbitrary machine with p_p=2 and p_c=3. From rotating-field theory it is known that a pulsating wave can be decomposed into two rotating waves in opposite direction. Following the same principle; the power- and control-winding main harmonic magnetic-field components, rotate in opposite direction from the rotor reference point of view. When super-imposed the resulting stator magnetic field will be a pulsating wave with radial frequency ω_{re}. As can be seen from figure 9, it is clear that the total stator magnetic field consists of 5 pulsating waves, with a pulse width equal to the pitch angle θ_{rp} of a rotor nested-loop. The 5 pulsating fields interact with the 5 nested-loops and by doing so induce currents in the rotor that produces a rotor magnetic field that opposes the stator magnetic field. A torque is then produced that forces the rotor in the direction of minimum energy. This is where the rotor current and torque are minimum. It can be concluded that the amplitude of the induced rotor currents and the torque production depend on the relative position angle γ_{shift} of the rotor to the stator magnetic field. This position angle

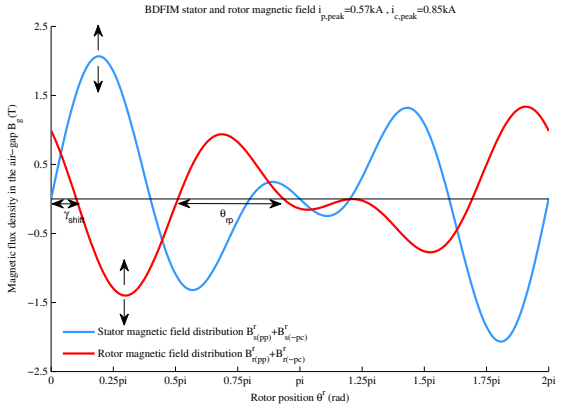

Fig. 9. Brushless DFIM stator and rotor magnetic field distribution, including the main harmonic field components.

can therefore be regarded as a load-angle. With minimum induced rotor current and torque generation at $\gamma_{shift} = \pi/(p_p+p_c)$. To change this load-angle, either the rotor can be shifted with an angle γ_{shift} or the stator magnetic field can be shifted by changing the angle between power and control winding currents $\varphi_p - \varphi_c$. For synchronous operation it is given that the voltages $u_{rp,nl(pp)}$ and $u_{rc,nl(-pc)}$ induced by the power- and control-winding main harmonic field components must match. Therefore, considering (23) the following equation must hold:

$$-p_p\gamma_{shift} - \varphi_p = p_c\gamma_{shift} - \varphi_c \tag{32}$$

Equation (32) can then be used to relate this load-angle to the angle between power- and control-winding currents:

$$\gamma_{shift} = \frac{\varphi_c - \varphi_p}{p_p + p_c} \tag{33}$$

When the load-angle between stator and rotor field is zero, the induced currents are maximum, however the produced torque is zero. The same applies when γ_{shift} is half a θ_{rp}, then the flux-linkage from the stator-field is minimum and therefore the induced current in the rotor is minimum. Also the torque is zero. In this way the brushless DFIM operates like a synchronous machine, where torque production depends on the relative position of the stator and rotor magnetic field components.

B. Winding Space-Harmonics in the Brushless DFIM

The presence of winding space-harmonic components in electrical machines can cause torque ripple. Only space-harmonic components with the same pitch angle do interact with each other. The rotor nested-loop design is developed to couple effectively to two main-harmonic magnetic field components, produced by the power- and control-winding. The rotor winding therefore has a richer space-harmonic spectrum compared to a traditional stator-winding. This contributes to some undesirable side-effects in this machine-type. Only stator and rotor magnetic field components of the same space-harmonic order k do couple. When there is no coupling these rotor winding space-harmonic magnetic field components add up to the leakage inductance, as can be observed from (29). This analysis considers a common fundamental harmonic component, corresponding to a 2-pole wave, for both stator windings and the rotor nested-loop construction. This enables a simple evaluation of the machines space-harmonic field spectrum. Figure 10 displays a magnetic field space-harmonic spectrum. The spectrum includes the contribution of the winding space-harmonic components of the stator

magnetic field in blue, consisting of a power-winding with p_p=2 and q_p=3 and a control-winding with p_c=3 and q_c=2. Further, the rotor winding space-harmonic components are displayed in red. The rotor consists of 5 nests with each 2 loops. From figure 10 it is obvious that the main space-harmonic components of both stator and rotor are $k=p_p$ and $k=-p_c$. Further, the space-harmonic components responsible for the production of ripple torque are indicated. These are in correspondence with the set of torque producing winding space-harmonics provided in (31).

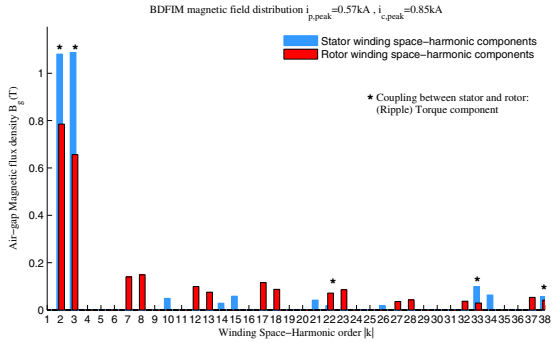

Fig. 10. Stator and rotor magnetic field distribution: winding-space harmonics

V. CONCLUSION

This paper provides a detailed analytical magnetic field model for the brushless DFIM. The analytical development shows that the brushless DFIM nested-loop rotor construction can be considered as a system of multiple poly-phase windings, therefore rotating-field theory can be applied in the model development. The number of rotor phases is equal to the number of nests. The number of separate rotor poly-phase windings is equal to the number of loops per nest. Further, harmonic analysis is applied to determine the contribution of winding space-harmonic components to the production of ripple torque. By considering a common fundamental harmonic component for both the power- and control-wining and the rotor-windings, a method is derived for identifying the winding space-harmonic components responsible for torque ripple production.

The derived magnetic field model is validated by FE calculations. A comparison is made of the magnetic field flux-density distribution of a case study machine. Also the mean torque, derived from the magnetic field is compared. Both show good accuracy.

Using the developed model the brushless DFIM operating principles are considered from a magnetic field point of view and a relation between current angles and rotor position with respect to the stator magnetic field is given.

The developed model is helpful for studying brushless DFIM operating principles and determining winding space-harmonic torque ripple components. However, the effects of saturation and slotting are neglected in this model.

VI. REFERENCES

[1] L.J. Hunt, "A New Type of Induction Motor", *Journal of the Institution of Electrical Engineers*, Vol.39, pp. 648-667, 1907.

[2] R. A. McMahon et al. ,"The BDFM as a Generator in Wind Turbines", *IEEE Power Electronics and Motion Control Conference*, 2006.

[3] A. E. Fitzgerald, C. Kingsley Jr., S. D. Umans, *Electric Machinery*, -6th ed., Mc Graw Hill, 2003.

[4] S. Williamson, A. C. Ferreira, A. K. Wallace, "Generalised theory of the brushless doubly fed machine. Part I : Analysis", *IEE Proc.-Electr. Power Appl.*, Vol. 144, NO. 2, March 1997.

[5] F. Blázquez et al. ,"Characterization of the Rotor Magnetic Field in a Brushless Doubly-Fed Induction Machine", *IEEE Trans. on Energy Conv.*, Vol.24, No.3, September 2009.

[6] S.Williamson,"Power-factr improvement incage-rotor induction motors", *Proc. IEE, Electr. Power. Appl.*, Vol.130, No.2, March 1983.

[7] P. C. Roberts, "A Study of Brushless Doubly-Fed Induction Machine (BDFM)", Ph.D. Dissertation, University of Cambridge, September 2004.

[8] E. Wiedenbrug et al. ,"Electromagnetic Mechanism of Synchronous Operation of the Brushless Doubly-Fed Machine", *Proc. Ind. Appl.Conf.*, vol. 1, October 1995.

[9] A. K. Wallace, P. Rochelle, R. Spée, "Rotor Modeling and Development for Brushless Doubly-Fed Machines", *ICEM – Conference record*, Vol.1, August 1990.

[10] J. Pyrhönen, T. Jokinen, V. Hrabovcová, *Design of Rotating Electrical Machines,* 1st ed., John Wiley & Sons, 2008.

VII. BIOGRAPHIES

Tim D. Strous received the M.Sc. degree in electrical engineering from Delft University of Technology, Delft, The Netherlands, in 2010.

Currently he is working towards the Ph.D. degree in the field of electrical machines. His current research interests include modelling and design of electrical machines.

Nils H. van der Blij graduated bachelors and masters from the technical University of Delft in 2011 and 2013 respectively.

His employment experience included Scarabee, Philips, and the Technical University of Delft. His special fields of interest are electrical machines and drives and sustainable energy generation.

Henk. Polinder (M'97, SM'13) received the M.Sc. and the Ph.D. degrees from Delft University of technology, Delft, the Netherlands, in 1992 and 1998. Since 1996 he has been an assistant/associate professor in the Electrical Power Processing Group of Delft University of Technology.

He worked part-time at Lagerwey in Barneveld in 1998/1999, at Philips Applied Technologies in Eindhoven in 2002 and at ABB Corporate Research in Vasteras in 2008. He was a visiting professor at the University of Newcastle-upon-Tyne in 2002, at Laval University, Quebec in 2004 and the University of Edinburgh in 2006.

He is author or co-author of over 200 papers. His research interests include design aspects of electrical machines, mainly for renewable energy applications.

J. A. (Bram) Ferreira (M'88, SM'01, F'05) received the B.Sc., M.Sc. and Ph.D. degrees in electrical engineering from Rand Afrikaans University, Johannesburg, South Africa, in 1981, 1983 and 1988, respectively, all in electrical engineering.

In 1981, he was with the Institute for Power Electronics and Electric Drives, Technical University, Aachen, Germany, and worked in industry at ESD (Pty) Ltd. From 1982 to 1985. From 1986 to 1997, he was with the Faculty of Engineering, Rand Afrikaans University, where he held the Carl and Emily Fuchs Chair of Power Electronics in later years. Since 1998, he has been a Professor at Delft University of Technology, Delft, the Netherlands.